Ice cliff slope stability analysis based on Fimbul granular ice properties

J.A.O. Econi, D. Kalumba, K. MacHutchon & S. Skatulla
University of Cape Town, Cape Town, South Africa.

ABSTRACT: This paper presents results obtained from material property investigations carried out on the Fimbul shelf ice, Antarctica, and their application to cliff stability analysis. Ice cores retrieved were observed to have a granular structure with occurrences of ice lenses. The granular structure was segmented into fine, medium and large grains, with medium grains in most abundance. The tested physical properties include density, elastic modulus and Poisson's ratio. Their average values were 569.9±157.7 kg/m^3, 1.66±0.87 GPa and 0.37±0.06, respectively. Strength properties tested were uniaxial compressive strength (UCS), shear and tensile strengths. The UCS test results had an average of 0.9±0.27 MPa, with ice made to fail in a ductile manner under a strain rate of $10^{-4.3}s^{-1}$. Shear strength was then determined using the rock mass rating characterisation based on ice - rock relationships identified. Classification of the samples resulted in cohesion and friction angle values of 0.25 MPa and 30º, respectively. Shear strength was further calculated as 0.77 MPa and tensile strength found equal to cohesion. These properties, applied to a finite element cliff model, output factors of safety (FS) ranging from 4.24 to 5.56. The cliff was therefore considered stable. However, further site surveys and deeper coring were recommended to model more representative shelf conditions.

1 INTRODUCTION

Antarctica is the southernmost continent globally and was the last to be discovered due to the harsh climatic conditions in the area. It houses about 90% of all the ice on earth and about 70% of all freshwater reserves (Campbell & Claridge 1987). The continent comprises bed rock, continental sheet ice, and ice shelves, which are year-round floating masses of ice attached to the sheet ice.

The Antarctic Treaty, signed in 1959, was aimed at preserving the continent's ecological systems (Turner et al. 2014). South Africa joined the treaty and oversees the South African National Antarctic Expedition IV (SANAE IV) research base in Antarctica. Annual voyages are carried out by ship from Cape Town to the Fimbul ice shelf to resupply the base. The shelf terminates at the ocean with a 28m vertical cliff, making offloading supplies and workforce only possible using the ship's deck crane.

Offloading onto the shelf has always been plagued by health and safety concerns raised due to cracks on the ice shelf surface. The concerns recently intensified into potential cliff instability worries due to the severity, frequency and orientation of cracks observed. An unstable cliff would significantly endanger the crew's lives on the shelf and damage the ship docked at the bottom of the cliff. This, therefore, warranted the need for a quantified stability analysis of the cliff.

Therefore, this study's main objective was to investigate the slope/cliff stability of the ice shelf cliff. Microscale, macroscale, and strength material properties were examined to perform the analysis. These parameters were then used as behavioural and characteristic inputs to the slope stability analysis.

2 METHODOLOGY

2.1 *Study area and research material*

The study area covered an approximate 200x100m area on the Fimbul ice shelf at 70º15'26.85"S 02º32'0.38"W. The longer 200m length was parallel to the shelf edge as illustrated in Figure 1.

Throughout this study, the material tested was ice retrieved from the Fimbul ice shelf, Antarctica. The ice used is termed as ordinary ice or Ih ice (Cole 2001) formed through snowfall metamorphism (Kinar & Pomeroy 2015) and sintering (White & McCallum 2018).

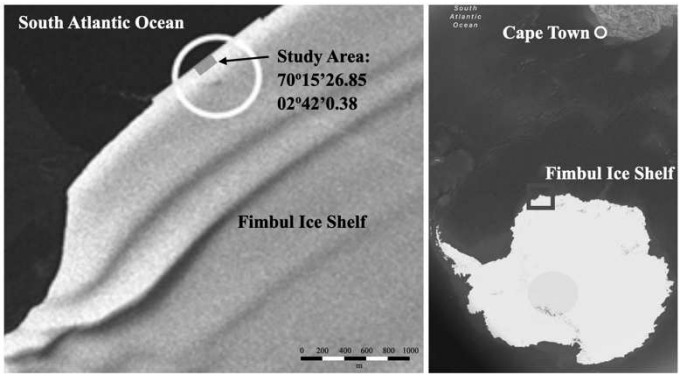

Figure 1. Study area location

2.2 *Sample collection and handling*

Before sample collection, site preparation was carried out. It involved the removal of all loose surface snow from the selected locations. Ice coring was then embarked to retrieve samples required for the study. A Mark II Kovacs ice corer was used. It had a 1 m height, a 90 mm diameter filament to hold ice cores, and length extensions for deeper coring. However, coring deeper than 1.5 m was avoided due to concerns of aggravated cliff instability.

Using the corer attached to a handheld Makita drill, 37 ice cores were retrieved from locations evenly distributed throughout the study area. Upon retrieval, these cores were stored in flexible PVC sleeves on which their coordinates and vertical orientations were indicated. All cores were then secured into insulated boxes and stored in the ship's freezer. After the voyage, a precooled freezer truck transported the cores from the harbour to the University of Cape Town polar lab. The cores were finally stored and processed inside the polar lab at -15±5ºC.

2.3 *Initial core assessments*

The initial core assessments that preceded all physical and strength tests were aimed at logging all available core information. These included length, coordinates, structural features, and transportation damages. Structurally, the cores were observed to be granular, with ice lenses occurring.

The rock quality designation (RQD) method was adopted to quantify the quality of the cores. Use of this method was motivated by the similarities between ice and rock in terms of formation processes (Jaeger et al. 2009, Petrovic 2003), material behaviour (Nguyen et al. 2017, Serré 2011), and testing methods (McCallum 2014, Lou & Wu 2022). An example of the similarities is that ice and rock exhibit viscoelastic deformation properties. Both have plastic deformation characteristics under low strain rates and confining pressures, and fracture mechanics under high strain rates and stress. Schulson (2001) also further emphasised the relationship by stating that a detailed understanding of rock aids in understanding ice as a material.

The RQD of each ice core was then calculated as a percentage of the sum of continuous lengths >10 cm to the total length of each core (Deere & Deere 1988). Discontinuities within the cores were determined to be changes in grainsize and positions of ice lenses. Transportation damages were ignored in the calculations.

2.4 *Morphology test procedures*

The morphology tests were aimed at further investigating the retrieved ice cores' structure. This investigation was carried out visually by placing ice cores onto an illuminated lightbox as illustrated in Figure 2. Variations in ice structure and grainsize were recorded using the lightbox. Sections with finer ice particles were observed to permit less light through them, with the amount of permitted light increasing with an increase in grainsize. This therefore led to the grainsize segmentation method adopted, similar to that used in MacDonell et al. (2021).

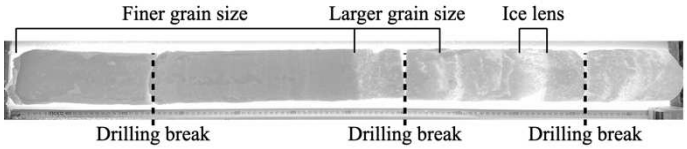

Figure 2. Core assessment on a lightbox

2.5 *Physical property test procedures*

Density, elastic modulus and Poisson's ratio were key physical properties required to model the ice material behaviour. Density was measured using the mass/volume method. This method was adopted due to its documented accuracy and ease of sample preparation. The complex porous granular ice structure made methods like hydrostatic weighting unfavourable for use (Pustogvar & Kulyakhtin 2016). A digital mass balance was used to measure the sample masses and vernier callipers used to obtain dimensions for volume calculations. Repeated measurements of each were carried out to reduce random errors (Hutchings et al. 2015).

Poisson's ratio and elastic modulus were both measured using dynamic ultrasound methods. A Proceq Pundit PL-200 with two 250 kHz shear wave transducers were used for the ultrasound tests as shown in Figure 3. The transducers measured the time taken for both pressure (P) and shear (S) waves through the material. Using the time taken, height of the samples, and density, elastic modulus and Poisson's ratio were calculated using the Equations 1, 2, and 3 below.

$$\nu = \frac{V_p{}^2 - 2V_s{}^2}{2(V_p{}^2 - V_s{}^2)} \quad (1)$$

$$G = \rho \times V_s{}^2 \quad (2)$$

$$E = 2G(1 + \nu) \quad (3)$$

where ν = Poisson's ratio, V_p = P wave velocity, V_s = S wave velocity, G = shear modulus, ρ = density, and E = elastic modulus.

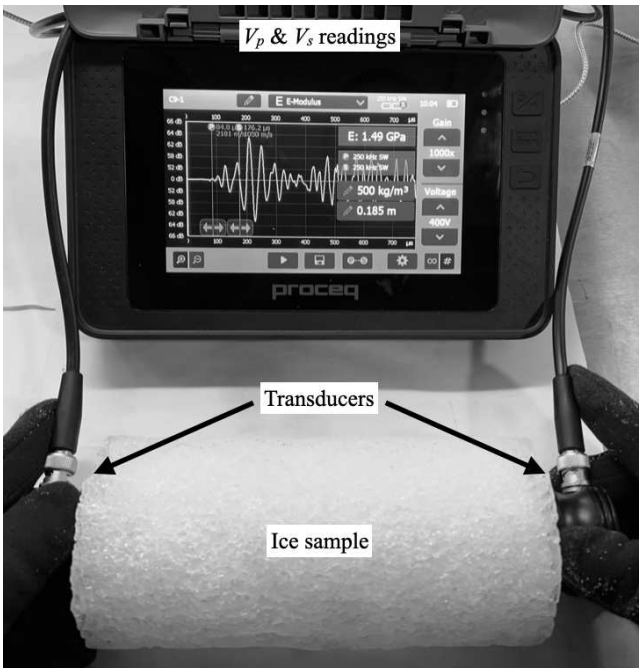

Figure 3. Ultrasound test equipment

2.6 *Strength property test procedures*

2.6.1 *Uniaxial compressive strength (UCS)*

The compression machine used for UCS was a GCTS PLT-2W. It is a lightweight, portable compression machine with a pneumatic system. Inhouse-designed stainless steel UCS platens were used.

Samples prepared for the compression tests were cut directly from the cores using a bandsaw. Samples were cut to heights >180 mm to be twice more significant than the sample diameters of 90 mm. Samples were placed between UCS platens, and the initial height of the sample (h_i) was measured using a vernier calliper as shown in Figure 4a). The compression test commenced with the load sensors plotting a load vs time graph as shown in Figure 4b).

The rate of loading was modulated to simulate slow snow accumulation on the ice shelves. The target strain rate was $<10^{-4}s^{-1}$ for ductile failure to occur (Cole 2001). Loading was maintained at this slow rate until the load sensors registered no further load increase. On completion of the tests, the final height of the sample (h_f) was measured and recorded. The strain rate used during each test was therefore calculated using Equation 4 below.

$$\Delta\varepsilon = \frac{h_i - h_f}{h_i \times \Delta t} \quad (4)$$

where $\Delta\varepsilon$ = strain rate, h_i = initial height, h_f = final height, and Δt = time.

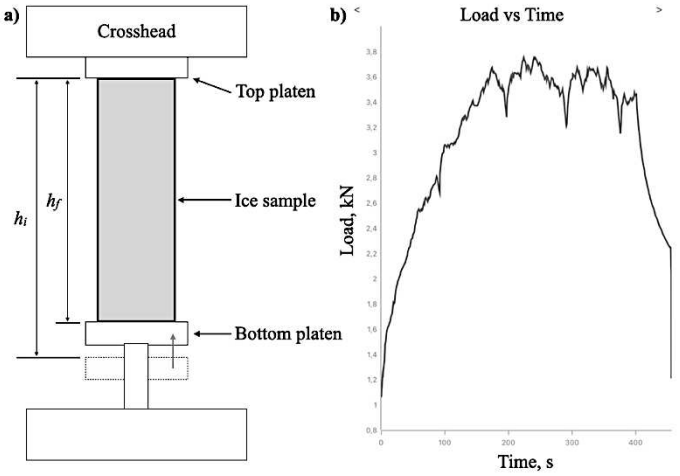

Figure 4. a) Compression test b) Load - time graph

2.6.2 *Shear strength*

The primary mechanisms with which ice masses were recorded to fail are fracture mechanics (Schulson 2001) and shear failure (Kulyakhtin & Høyland 2014). The latter is a frequently used method to define failure of ice masses with authors like Podolskiy et al. (2015) and Serré (2011) using the Mohr Coulomb shear failure criterion to model ice's failure characteristics. Therefore, using the Mohr-Coulomb method in this study, shear strength and its associated parameters, cohesion and friction angle, were required. The rock mass rating (RMR) method (Bieniawski 1979) was adopted to obtain these. This was due to the ice-rock relationships, low resource intensity, and method adaptability (Econi 2024).

The parameters used to determine the RMR of materials include RQD, UCS, discontinuity conditions, orientation and spacing, and groundwater conditions (Kundu et al. 2020). RQD, discontinuity spacing, and UCS values were obtained quantitatively from the results of their respective tests. The remaining three were assessed qualitatively by inspecting the conditions of the samples. Ground water conditions were decided by the unavailability of wetness during core retrieval on the ice shelf. Discontinuity conditions were then determined by the state of the interfaces between varying grain sizes and ice lenses, and discontinuity orientation by the angle of each discontinuity.

Each of the mentioned parameters was then assigned a rating, and their summation was given to the material. The total RMR value gave an RMR class for the ice, which was used to obtain a range of cohesion and friction angle values to represent the material's shear strength properties. The shear strength of the material was therefore calculated using Equation 5 below.

$$\tau = c + \sigma' tan\phi \quad (5)$$

where τ = shear strength, c = cohesion, σ' = effective normal stress from UCS, and ϕ = angle of friction.

2.7 *Shelf modelling*

Material properties from the tests were applied as input parameters for cliff stability modelling. Rocscience's RS2 Finite Element Modelling (FEM) software was used for its capabilities in modelling complex materials, low resource intensity, and application of the Shear Reduction Factor (SRF).

The model was built as a 100 m thick ice shelf (Nøst 2004) with a 90º shelf edge/ice cliff. The model was extended 200 m inland to encompass the entire study area, and a sea level was placed 28 m below the surface and against the vertical cliff.

Three material layers were modelled into the cliff. These were granular ice, upper firn, and lower firn layers, as illustrated in Figure 5. Firn ice is a transitional ice stage between snow and glacial ice. The granular ice layer was modelled from the shelf surface to 20 m depth (MacDonell et al. 2021) with properties from laboratory tests. The lower firn layer, from 50 m to 100 m depth, was modelled as crystalline ice with properties obtained from deep core drilling and tests (Petrovic 2003, White & McCallum 2018, Schulson 2001, Bassis & Walker 2012, Yasui et al. 2017). From 20 m to 50 m, the upper firn layer was finally added as a transitional layer to provide a linear transition of material properties (Rist et al. 2002) from the granular layer to crystalline ice.

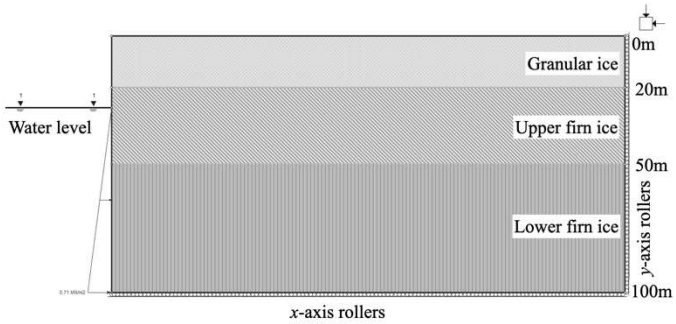

Figure 5. Ice shelf model

A base model with the structure in Figure 5, was run to observe the slope stability characteristics in an ideal shelf scenario without cracks or discontinuities. A 3 m deep and 1 m wide crack was added to the model to test the influence of crack distance from the shelf edge. All models were run using a 6 node triangular graded mesh, with a minimum of 16500 elements where convergence occurred.

3 RESULTS AND DISCUSSIONS

3.1 *Core characterisation*

Granular ice sections of the cores were segmented into fine, medium and large grain sizes, as illustrated in Figure 6. Each occupied 19.7%, 62.4% and 17.9% of the total granular ice, respectively. This segmentation method was similarly adopted by MacDonell et al. (2021). The arrangement of grain sizes for ice core depth was observed to be random, with each grainsize occurring at no specific depth or quantity.

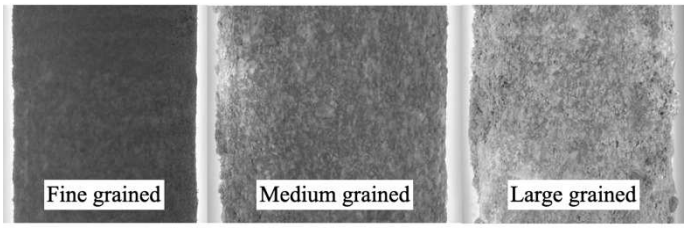

Figure 6. Grainsize segmentation

The variation of grainsize percentages was attributed to the process of metamorphism that occurs from snow to fine-grained ice, medium, large, then non-granular crystalline ice. With the metamorphism caused due to the pressure of overburdened snow/ice and temperature fluctuations (Ligneau et al. 2022), the transition from fine to medium ice required less metamorphism than the transition from medium to sizeable large-grained ice. This explained the more extraordinary occurrence of medium-grained ice on the shelf.

The average densities of each segmented grain size were 473.2 kg/m^3, 469.7 kg/m^3, and 406.2 kg/m^3 for fine, medium and large grain sizes, respectively. The trend observed was a reduction in density with an increase in grainsize. This was attributed to porosity and air pockets within the larger grain-sized ice. An additional average density for samples containing a mix of grainsizes and ice lenses was 564.1 kg/m^3. These samples were referred to as mixed samples.

Ice lenses created were observed from rainwater seepage and recrystallisation of meltwater inside the granular ice. The percentage of ice lenses on cores ranged from 0% to 33.6% and had density measurements of 813.0 kg/m^3. The difference between the ice lens density and 920 kg/m^3 of crystalline ice (White & McCallum 2018) was attributed to trapped air and granular ice within ice lenses.

RQD measurements ranged between 43% and 100% on all retrieved cores. As the measurement was intended to represent a homogenous ice material for modelling, a mean RQD was calculated. The value of 76±14.5% was statistically obtained using the normal distribution to represent the entire material, as shown in Figure 7a.

The mean RQD value would have the impact of installing the effects of discontinuities caused by changes in grainsize and occurrences of ice lenses within the homogenous material to be modelled for slope stability analyses.

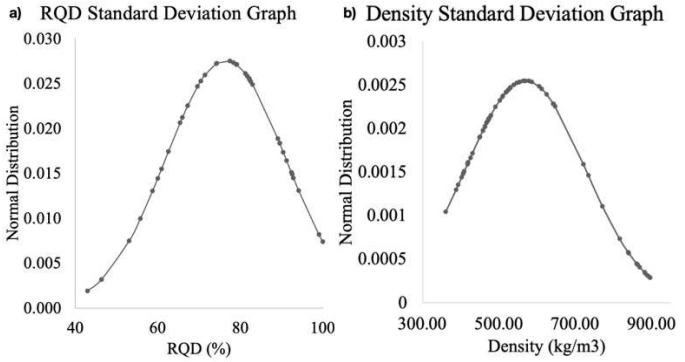

Figure 7. a) RQD; b) Density standard deviation curves

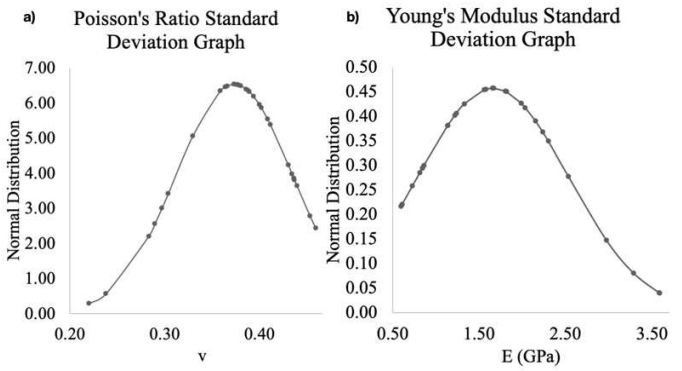

Figure 8. a) Poisson's ratio b) Elastic modulus standard deviation curves

3.2 *Physical property results and analysis*

Similar to RQD, density measurements were required to represent a homogenous material for modelling purposes. A mean density of 569.9±157.5 kg/m^3 was calculated. The value encompassed all measurement random errors as shown in Figure 7b. The value obtained was relatable to the density of mixed samples and was therefore confirmed to be representative of the accurate composition of the material.

Results from the ultrasound tests gave V_p and V_s values in the ranges of 1852 m/s to 3354 m/s and 712 m/s to 1640 m/s respectively. These ranges were used to calculate Poisson's ratio using Equation 1 to the ranges of 0.22 to 0.44. The mean value representing the homogenous ice material was, therefore, 0.37±0.06 as shown in Figure 8a. Compared to what has been documented in the literature, Sinha (1989) and Petrovic (2003) each obtained v as 0.31 and 0.29 - 0.32, respectively for crystalline ice. This, therefore, illustrated that granular ice on the shelf showed higher deformation characteristics than crystalline ice.

With the v values obtained, values of E were calculated using Equation 3 to a range of 0.61 GPa to 3.19 GPa for all samples. These resulted in a statistical mean of 1.66±0.87 GPa for the homogenous ice as shown in Figure 8b. When compared to the other ice types, Petrovic (2003) & Yasui et al. (2017) obtained E crystalline values ice between 9.7 GPa and 11.2 GPa. In contrast, Serré (2011) & Ligneau et al. (2022) obtained E values for snowpack between 0.7 MPa and 1.14 MPa. Therefore, the obtained value of 1.66±0.87 GPa showed that granular ice was significantly stiffer than snowpack but less stiff than crystalline ice.

3.3 *Strength property results and analysis*

3.3.1 *UCS and strain rates*

The samples selected for UCS tests were mixed samples cut to heights >180 mm. These mixed samples were chosen because their density closely matched the overall density of the ice material.

Failure loads measured by the compression machine ranged from 2.20 kN to 8.28 kN. When divided by the cross-sectional areas of the samples, these equated to 0.37 - 1.33 MPa stresses. To obtain a value for the homogenous material, the mean UCS was calculated to be 0.9±0.27 MPa. This strength was found to be comparable to the 1.2 - 1.7 MPa strengths of laboratory-made snow in Wang et al. (2021), but significantly weaker than crystalline ice strengths of 4 MPa to 30 MPa (Rist et al. 2002).

During the compression tests, failure was observed to occur in a ductile manner as samples axially deformed under load application. The average strain was $10^{-4.3}s^{-1}$, within the ductile failure range of $<10^{-3}s^{-1}$ (Shazly et al. 2009).

During the deformation, the sound of microcracks was audible, indicating the failure of freeze bonds within the material. Despite this, the overall structure of the samples was maintained due to the sintering and compaction of grains into the previously empty air voids within the sample.

3.3.2 *Shear strength and tensile strength*

Each of the parameters in the RMR method had a result used to obtain the overall RMR rating of the material. For the qualitative parameters, firstly, interfaces between discontinuities were rated as slickensides due to slipperiness between layers when melting occurs. Secondly, groundwater conditions were rated as dry due to the unavailability of water during core removal. Third, discontinuity orientations were flat throughout all retrieved cores. These results and their associated RMR number are summarised in Table 1 below.

Table 1. Rock mass rating results

Parameter	Result	RMR Rating
RQD (%)	76.0±14.5	17
UCS (MPa)	0.90±0.27	0
Discontinuity spacing (mm)	97	8
Discontinuity condition	Slickensides	10
Discontinuity orientation (º)	0	-0
Groundwater	Dry	15
Sum		50

The summation of all parameter results was 50, which, according to Bieniawski (1979), falls within the range of 41 - 60 for class III materials. The shear strength parameters, cohesion and friction angle for material class III are 0.2 - 0.3 MPa and 25º - 35º, respectively. With the RMR value of 50, the shear parameters representing the material were, therefore, 0.25 MPa and 30º, respectively.

Compared to various ice types tested, the cohesion value selected lies between 2.5 kPa of snowpack (Podolskiy et al. 2015) and 1 MPa of glacier ice (Bassis & Walker 2012). This spectrum of cohesion strengths was justified by the increasing metamorphism from snowpack to granular ice and glacial ice. Similarly, snowpack was tested to have a friction angle range of 12º to 28º (Reiweger et al. 2015), while crystalline ice ranged from 30º to 45º (Schulson 2001).

The shear strength of the ice material was therefore calculated using Equation 5. With the effective normal stress equal to the UCS test result of 0.9 MPa, the shear strength calculation resulted in a value of 0.77 MPa.

Tensile strength was finally defined as the bond strength between ice particles, which is also the definition of cohesion in ice (Podolskiy et al. 2015). Due to this, the tensile strength was equated to the cohesion value of 0.25 MPa.

3.4 *Model results*

Failure in the models occurred when instability through excessive deformation was detected. The SRF at which this happened was labelled as the failure SRF. Due to the tolerance setting of 0.01, the SRF 0.01 less than the failure SRF was labelled as the critical SRF.

For the base scenario, the model output a critical SRF value of 5.56 and a failure SRF of 5.57, as observed in Figure 9. Failure was observed to occur in shear through a shear plane originating from about 60 m inland to a depth of 40 m at the cliff edge as shown in Figure 9b. Tensile failures were also observed on the shelf's surface, which eluded to the formation of crevasses (Rist et al. 2002).

During the horizontal variation of the crack discontinuity, a critical range with the lowest SRFs was observed between 9 m and 20 m from the shelf edge. This range had the lowest SRF values between 4.24 and 4.40, with the lowest existing at 13 m with a critical SRF of 4.24 and failure SRF of 4.25.

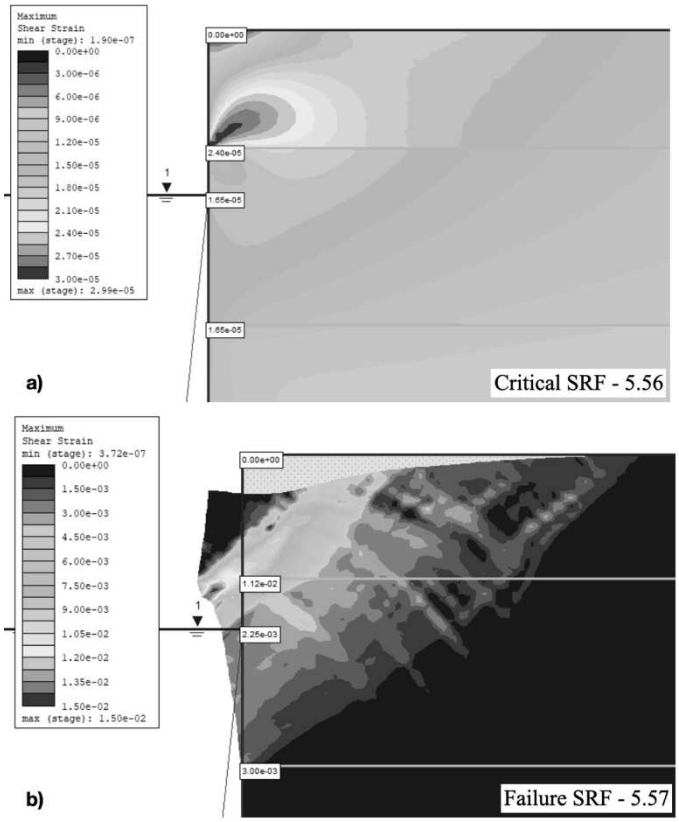

Figure 9. a) Critical SRF; b) Failure SRF base model outputs

At the critical SRF, tensile failures were observed at the bottom of the introduced crack, as highlighted in Figure 10a. This was attributed to continued crack propagation as the tensile forces exceeded the material's tensile strength (Schulson 2001). This was observed to be more representative behaviour of ice shelves as seen in Figure 10b). It was also noted that deepening of cracks introduced the possibility of toppling failure through formation of toppling blocks (Scambos et al. 2009). At the failure SRF, shear failure was also observed similar to the base scenario, with an origin influenced by the position of the crack.

4 CONCLUSION AND RECOMMENDATIONS

The properties investigated in this study sufficiently described the physical nature of the Fimbul granular ice and provided behavioural characteristics of the material.

The SRFs of the shelf models output values ranging between 4.24 and 5.56, which show a stable ice cliff. These results agree with the ice cliff's current non-failed state.

However, it is recommended that deeper coring for accurate material layer properties and a more detailed survey of the cracks on the shelf be carried out. This

would provide more precise locations and depths of cracks to model more representative shelf conditions.

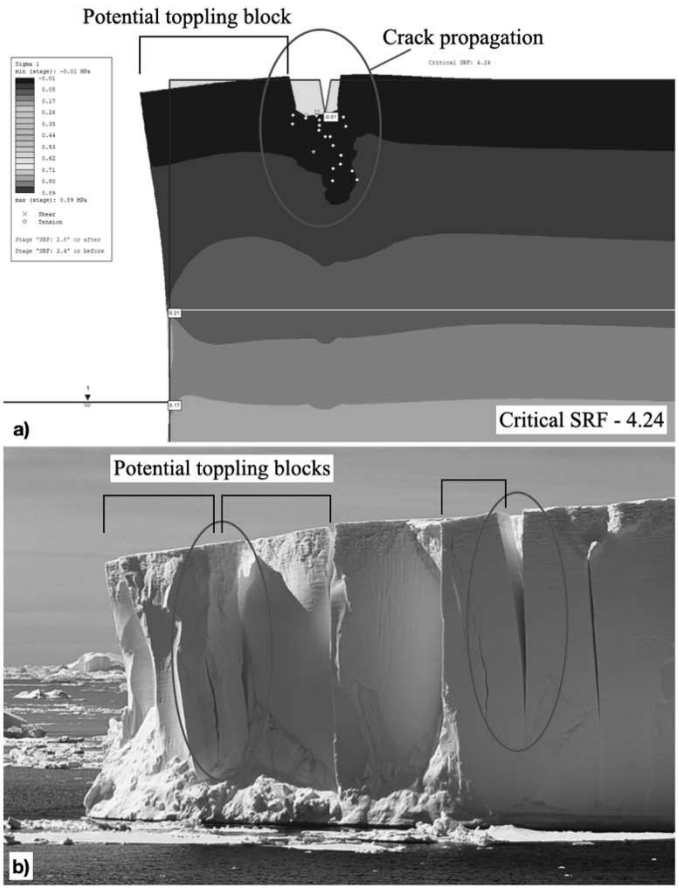

Figure 10. a) 13m Critical SRF output; b) Ice toppling blocks (Pollard & DeConto, n.d.)

REFERENCES

Bassis, J.N. & Walker, C.C. 2012. Upper and lower limits on the stability of calving glaciers from the yield strength envelope of ice. *Proceedings of the Royal Society A: Mathematical, Physical and Engineering Sciences* 468(2140): 913-931.

Bieniawski, Z. Ed. 1979. *The geomechanics classification in rock engineering applications*. OnePetro.

Campbell, I.B. & Claridge, G.G.C. 1987. *Antarctica: soils, weathering processes and environment*. Elsevier.

Cole, D.M. 2001. The microstructure of ice and its influence on mechanical properties. *Engineering fracture mechanics*. 68(17-18): 1797-1822.

Deere, D. & Deere, D. Eds. 1988. The rock quality designation (RQD) index in practice.

Econi, J.A.O. 2024. Investigated Physical/Strength Properties and Elastic Constants of Fimbul Granular Ice Applied to Ice Cliff Stability Analysis. *MSc Dissertation*. University of Cape Town.

Hutchings, J.K., Heil, P., Lecomte, O., Stevens, R., Steer, A. & Lieser, J.L. 2015. Comparing methods of measuring sea-ice density in the East Antarctic. *Annals of Glaciology* 56(69): 77-82.

Jaeger, J.C., Cook, N.G. & Zimmerman, R. 2009. *Fundamentals of rock mechanics*. John Wiley & Sons.

Kinar, N. & Pomeroy, J. 2015. Measurement of the physical properties of the snowpack. *Reviews of Geophysics* 53(2): 481-544.

Kulyakhtin, S. & Høyland, K.V. Eds. 2014. Study of the volumetric behaviour of ice rubble based on bi-axial compression data. *American Society of Mechanical Engineers*. V010T007A027.

Kundu, J., Sarkar, K., Singh, A.K. & Singh, T. 2020. Continuous functions and a computer application for Rock Mass Rating. *International Journal of Rock Mechanics and Mining Sciences* 129: 104280.

Ligneau, C., Sovilla, B. & Gaume, J. 2022. Numerical investigation of the effect of cohesion and ground friction on snow avalanches flow regimes. *Plos one* 17(2): e0264033.

Lou, X. & Wu, Y. 2022. Influence of temperature and fiber content on direct shear properties of plain ice and fiber-reinforced ice. *Cold Regions Science and Technology* 194: 103458.

MacDonell, S., Fernandoy, F., Villar, P. & Hammann, A. 2021. Stratigraphic analysis of firn cores from an Antarctic ice shelf firn aquifer. *Water* 13(5): 731.

McCallum, A. 2014. Cone penetration testing (CPT) in Antarctic firn: an introduction to interpretation. *Journal of Glaciology* 60(219): 83-93. DOI:10.3189/2014JoG12J214.

Nguyen, N.H., Bui, H.H., Nguyen, G.D. & Kodikara, J. 2017. A cohesive damage-plasticity model for DEM and its application for numerical investigation of soft rock fracture properties. *International Journal of Plasticity* 98: 175-196.

Nøst, O.A. 2004. Measurements of ice thickness and seabed topography under the Fimbul Ice Shelf, Dronning Maud Land, Antarctica. *Journal of Geophysical Research:* Oceans 109(C10).

Petrovic, J.J. 2003. Review Mechanical properties of ice and snow. *Journal of Materials Science* 38(1): 1-6. DOI:10.1023/A:1021134128038.

Podolskiy, E.A., Chambon, G., Naaim, M. & Gaume, J. 2015. Evaluating snow weak-layer failure parameters through inverse finite element modelling of shaking-platform experiments. *Natural Hazards and Earth System Sciences* 15(1): 119-134.

Pollard, D. & DeConto, R. n.d. The birth and death of ice sheets: Understanding the past and predicting the future.

Pustogvar, A. & Kulyakhtin, A. 2016. Sea ice density measurements. Methods and uncertainties. *Cold Regions Science and Technology* 131: 46-52.

Reiweger, I., Gaume, J. & Schweizer, J. 2015. A new mixed-mode failure criterion for weak snowpack layers. *Geophysical research letters* 42(5): 1427-1432.

Rist, M., Sammonds, P., Oerter, H. & Doake, C. 2002. Fracture of Antarctic shelf ice. *Journal of Geophysical Research: Solid Earth* 107(B1): ECV 2-1-ECV 2-13.

Scambos, T., Fricker, H.A., Liu, C.-C., Bohlander, J., Fastook, J., Sargent, A., Massom, R. & Wu, A.-M. 2009. Ice shelf disintegration by plate bending and hydro-fracture: Satellite observations and model results of the 2008 Wilkins ice shelf break-ups. *Earth and Planetary Science Letters* 280(1-4): 51-60.

Schulson, E.M. 2001. Brittle failure of ice. *Engineering fracture mechanics* 68(17-18): 1839-1887.

Serré, N. 2011. Mechanical properties of model ice ridge keels. *Cold Regions Science and Technology* 67(3): 89-106.

Shazly, M., Prakash, V. & Lerch, B.A. 2009. High strain-rate behavior of ice under uniaxial compression. *International Journal of Solids and Structures* 46(6): 1499-1515. DOI: https://doi.org/10.1016/j.ijsolstr.2008.11.020.

Sinha, N.K. 1989. Elasticity of natural types of polycrystalline ice. *Cold Regions Science and Technology* 17(2): 127-135.

Sinha, N.K. & Shokr, M. 2015. *Sea ice: physics and remote sensing*. John Wiley & Sons.

Turner, J., Barrand, N.E., Bracegirdle, T.J., Convey, P., Hodgson, D.A., Jarvis, M., Jenkins, A. & Marshall, G. et al. 2014.

Antarctic climate change and the environment: an update. *Polar record* 50(3): 237-259.

Wang, E., Fu, X., Han, H., Liu, X., Xiao, Y. & Leng, Y. 2021. Study on the mechanical properties of compacted snow under uniaxial compression and analysis of influencing factors. *Cold Regions Science and Technology* 182: 103215.

White, G. & McCallum, A. 2018. Review of ice and snow runway pavements. International *Journal of Pavement Research and Technology* 11(3): 311-320.

Yasui, M., Schulson, E.M. & Renshaw, C.E. 2017. Experimental studies on mechanical properties and ductile-to-brittle transition of ice-silica mixtures: Young's modulus, compressive strength, and fracture toughness. *Journal of Geophysical Research: Solid Earth* 122(8): 6014-6030.